RSC Advances

PAPER

View Article Online
View Journal | View Issue

Cite this: *RSC Adv.*, 2020, **10**, 21822

Application of polyethylenimine-coated magnetic nanocomposites for the selective separation of Cs-enriched clay particles from radioactive soil†

June-Hyun Kim,[ab] Sung-Man Kim,[a] In-Ho Yoon [a] and Ilgook Kim *[a]

The separation of Cs-enriched fine particles is a highly effective way to reduce the volume and radioactivity of contaminated soil. This work demonstrated the application of polyethylenimine (PEI)-coated Fe_3O_4 nanocomposites and a mesh filter for the selective separation of clay particles from Cs-contaminated soil. The PEI coating on the Fe_3O_4 nanoparticles enhanced the binding force between the magnetic nanoparticles and clay minerals *via* electrostatic attraction; thus, approximately 100% of the clay particles were magnetically separated from solution by Fe_3O_4-PEI nanocomposites at a low dose (0.04 g-nanocomposite per g-clay). In separation experiments with soil mixtures, clay- and silt-sized fine particles that had been magnetized by Fe_3O_4-PEI nanocomposites were selectively separated, and the separation efficiency improved when a mesh filter was added to exclude physically large particles. The combination of magnetic and sieving separation thoroughly separated fine particles from soil by reducing the volume of the magnetic fraction. We also evaluated the magnetic-sieving separation method for the selective removal of clay particles from ^{137}Cs-contaminated soil. The decrease in radioactivity in the treated nonmagnetic fraction, which accounted for 87.5% of the total soil, corresponded to a high decontamination efficiency of approximately 90%. The developed separation technology offers great potential for the efficient remediation of radioactive soil.

Received 17th April 2020
Accepted 28th May 2020

DOI: 10.1039/d0ra03426f

rsc.li/rsc-advances

Introduction

After the Fukushima Daiichi Nuclear Power Plant accident in 2011, a large amount of radioactive cesium was released into the surrounding environment, resulting in severe soil contamination.[1] In particular, ^{137}Cs deposited in soil is the primary source of threat, because it has a relatively long half-life (30.1 years) and the potential for long-term exposure to gamma rays from increased ambient air dose rates or through ingestion of food products of the contaminated area.[2] Since most cesium remains within the top 10 cm of soil, topsoil scraping was an essential way to reduce the radioactivity in the contaminated area.[3] A substantial amount of radioactive soil waste, with an estimated volume of approximately 18.7–28 million m^3, is stored at temporary storage sites.[3] Therefore, it is necessary to develop effective and efficient techniques to reduce the volume of Cs-contaminated soil waste.[5]

Generally, the migration and retention of Cs in soil are predominantly controlled by micaceous clay minerals.[6–11] In Fukushima soil, weathered biotite, an effective Cs sorbent, is a major component of various clay minerals.[12,13] Compared with other clay minerals, weathered biotite contains more Cs-specific sorption sites, such as interlayer or frayed edge sites (FES), revealing high Cs affinity *via* inner-sphere complexation.[11,14,15] The Cs adsorbed on FES diffuses into deeper into the interlayers by Cs dehydration and then readily exchanges with neighboring K. Consequently, this trapped Cs is difficult to remove from clay because it is tightly bound in between two tetrahedral sheets.[4,16,17]

For the contaminated soil in Fukushima, it has been reported that the <5 μm size fraction accounts for approximately 7% of the topsoil (0–10 cm); the Cs distribution is higher in this fraction than in silt and sand, which make up the majority of the rest of the topsoil.[18] For this reason, the removal of fine particles could lower radioactivity of the remaining soil. Nakanishi *et al.* (2016)[19] reported that radioactivity was reduced by more than 80% after the separation of suspended clay from a mixed soil suspension. Therefore, the separation of clay containing a high concentration of Cs from soil can be an effective strategy for radioactive soil decontamination. Several chemical/physical methods have been reported for the separation of Cs-contaminated clay. For example, flotation technology was applied for the selective separation of Cs-contaminated clays.

[a]*Decommissioning Technology Research Division, Korea Atomic Energy Research Institute, 111, Daedeok-daero 989 Beon-gil, Yuseong-gu, Daejeon, 305-353, Republic of Korea. E-mail: ilgook@kaeri.re.kr; Tel: +82-42-868-2495*

[b]*School of Architectural, Civil, Environmental, and Energy Engineering, KyungPook National University, 80 Daehak-ro, Sangyeok-dong, Buk-gu, Daegu, Republic of Korea*

† Electronic supplementary information (ESI) available. See DOI: 10.1039/d0ra03426f

Said *et al.* (2019)[20] employed a continuous particulate froth flotation process using a cationic surfactant to separate negatively charged fine soil particles (<100 μm). Zhang *et al.* (2019)[21] also studied the froth flotation method to selectively separate Cs-loaded clays from uncontaminated clays. In addition, magnetic separation has been used to separate contaminated clay. Igarashi *et al.* (2014)[22] separated 2 : 1-type clay minerals with paramagnetic properties from soil particles using a superconducting magnet. Mallampati *et al.* (2015)[23] synthesized and applied Fe/Ca/CaO/[PO_4] nanocomposites for magnetic separation and immobilization of Cs in dry contaminated soil. To date, few techniques have been reported for the separation of clay particles from soil, and their practical applications are still limited in terms of separation efficiency (SE).

In our recent research,[24] we used Fe_3O_4 nanoparticles coated with cationic polymers for the selective separation of Cs-contaminated illite clay from soil based on the negative charge of the clay surface. Due to the selective sorption of the cationic Fe_3O_4 nanocomposites onto clay particles through electrostatic attraction, ^{137}Cs-contaminated clay could be effectively and readily separated from a soil mixture. However, clay particles and silt- or sand-sized particles with a low Cs concentration were also separated to some extent by the magnetic nanocomposites. Therefore, to increase the selectivity of clay particle separation, we added a mesh filter for physical separation. The combination of magnetic and sieving methods can more selectively separate clay particles by excluding larger magnetic particles from passing through the mesh filter. Thus, we investigated the effects of sieving and nanocomposite dose on the SE of fine particles based on the particle size distribution. In addition, the reduction in volume and radioactivity of ^{137}Cs-contaminated soil by magnetic separation were evaluated.

Materials and methods

Materials

Hydrobiotite (HBT) obtained from Sigma-Aldrich was used as the clay substrate after being ground in a milling machine and sieved through a 20 μm mesh. Other clay minerals, including illite (Yong Koong Illite Co., Korea), kaolinite (Sigma-Aldrich) and montmorillonite (Clay Minerals Repository, USA), were used for comparison. A soil sample was collected near the site of the Korea Atomic Energy Research Institute (KAERI), Daejeon, Korea, and was used after being sieved to a size of less than 2 mm and then dried at room temperature for one week.

Synthesis of Fe_3O_4-PEI nanocomposites

First, Fe_3O_4 nanoparticles were prepared by chemical coprecipitation.[25] $FeCl_2 \cdot 4H_2O$ (2.01 g) and $FeCl_3$ (3.34 g) were dissolved in 100 mL of DI water in a four-neck flask and heated at 80 °C under a nitrogen atmosphere. After the addition of 23 mL of NH_4OH (28–30%) into the solution, the mixture was stirred continuously for 30 min. The resulting magnetic nanoparticles were separated from the mixture using a permanent NdFeB magnet (0.38 T, 5 × 5 × 2.5 cm, JL Magnet, Korea) and then washed 5 times with DI water.

Then, PEI-coated Fe_3O_4 nanocomposites were synthesized by adding a 5 wt% PEI solution ($M_w \approx 25$ kDa) to the Fe_3O_4 nanoparticles at a mass ratio of 0.1 : 1 g-PEI per g-Fe_3O_4 nanoparticles, and the mixture was sonicated for 1 h. The nanocomposites were collected from the solution using a permanent magnet and then washed 5 times with DI water. The Fe_3O_4-PEI nanocomposites were dispersed in DI water for further use.

Interaction between the Fe_3O_4-PEI nanocomposites and clay minerals

To magnetically separate clay minerals from solution, Fe_3O_4-PEI nanocomposites were mixed for 15 min with HBT (50 mg) at various mass ratios (0.005 : 1, 0.02 : 1, 0.04 : 1, 0.08 : 1, and 0.1 : 1 g-nanocomposite per g-clay mineral) in 17 mL of DI water in a 20 mL glass bottle. For comparison, Fe_3O_4-PEI nanocomposites were also mixed with kaolinite, montmorillonite, and illite at a mass ratio of 0.02 g-nanocomposite per g-clay mineral. After mixing, a permanent magnet was placed next to the bottle for 3 min to separate the nanocomposite–clay mineral complexes. The separation efficiency (SE%) of clay from solution was calculated using the equation $SE\% = [1 - (M_r/M_t)] \times 100\%$, where M_r and M_t are the clay mass in the solution before and after magnetic separation. The weight of each clay particle in the solution was measured after being completely dried in a vacuum oven.

Selective separation of fine particles from a soil mixture

The magnetic separation experiments were performed using a soil mixture of 90% sand and 10% clay (HBT, mean size: 7 μm) in a 500 mL open acrylic chamber. To combine sieve separation with magnetic separation, a mesh filter (0.075 mm) was inserted vertically into the chamber. The Fe_3O_4-PEI nanocomposites were mixed for 10 min with 10 g of soil mixture in 250 mL of DI water at various mass ratios (0.04 : 1, 0.08 : 1, 0.12 : 1, and 0.16 : 1 g-nanocomposite per g-HBT). After mixing, the soil mixture containing the Fe_3O_4-PEI nanocomposites was separated under a magnetic field, and the particle size distributions of the nonmagnetic and magnetic soil fractions were analyzed. Each soil sample was divided into five fractions—sand (2.0–0.5, 0.5–0.2, and 0.2–0.075 mm), silt (0.075–0.038 mm), and silt–clay (<0.038 mm)—according to the AASHTO soil classification system.

To evaluate the efficiency of the reduction in radioactivity by magnetic-sieving separation, radioactive $^{137}Cs^+$-sorbed soil was prepared by mixing soil (100 g) with 1 L of an aqueous Cs^+ solution (220 Bq L^{-1}) for 7 days at room temperature. The radioactivity of the $^{137}Cs^+$-sorbed soil was 2152 Bq kg^{-1}. Fine particles less than 0.038 mm accounted for approximately 8.5% of the contaminated soil. The experimental procedure was conducted at a mass ratio of 0.12 g-nanocomposites per g-fine particles by using the same procedures described above. The efficiency of the reduction in radioactivity in the $^{137}Cs^+$-sorbed soil was determined using the equation $RE\% = [1 - (R_n/R_i)] \times 100\%$, where R_i and R_n are the radioactivity of the initial soil and nonmagnetic soil.

Analytical methods

The morphology of the Fe_3O_4-PEI nanocomposites and HBT–nanocomposite complexes was observed by ultracorrected energy-filtered transmission electron microscopy (UC-EF-TEM, Carl Zeiss, Germany). Thermogravimetric analysis (TGA, Mettler-Toledo, USA) was performed to confirm the amount of PEI coating using a LABSYS Evo (Setaram, France) under a nitrogen atmosphere at a heating rate of 30 °C min^{-1}. Attenuated total reflection Fourier transform infrared (ATR-FTIR) spectroscopy was also conducted using an iS5 spectrometer (Thermo, USA) to analyze the functional groups of the Fe_3O_4-PEI nanocomposites. For the zeta potential measurements, 10 mg sample was transferred to 10 mL DI water. The pH of the solution was measured with an Orion pH electrode (Thermo, USA) and adjusted by dropwise addition of 0.1 M HCl and NaOH. After adjusting the pH of the solution, the zeta potentials of the nanocomposites and clay minerals were analyzed by dynamic light scattering (DLS) using a Nano-Zs90 zetasizer (Malvern, UK). Each measurement was the average of 100 measurements and the entire experiment was conducted in triplicate. For measurement of radioactivity, initial and nonmagnetic soil samples were analyzed using gamma spectrometry with a multichannel analyzer (MCA; Canberra, USA) that has a high purity germanium (HPGe) detector. The specific activity of ^{137}Cs was determined by measuring its gamma-ray at 661.6 keV. The activity of ^{137}Cs in the samples was evaluated using the total net counts under the selected photopeak, applying gamma intensity of the radionuclide and weight of the sample. The radioactivity concentration was expressed as Bq kg^{-1}.

Results and discussion

Characteristics of the Fe_3O_4-PEI nanocomposites

Amino-functionalized magnetic nanocomposites were synthesized based on the surface characteristics of clay particles. A TEM image of the Fe_3O_4-PEI nanocomposites shows relatively uniform spherical morphologies and an average size of approximately 10 nm (Fig. 1a). Surface modification of the Fe_3O_4 nanoparticles with PEI was confirmed through FTIR analysis and TGA. As shown in Fig. S1,† strong adsorption peaks

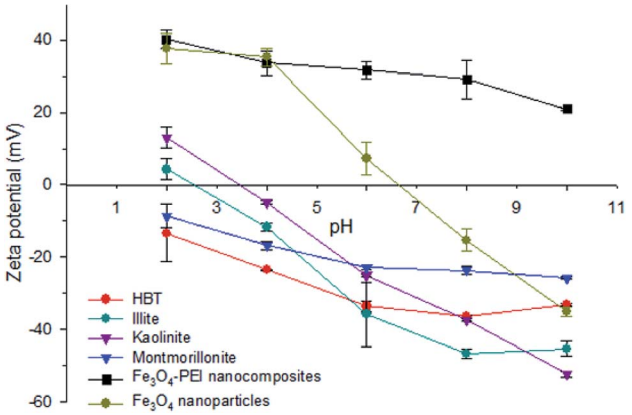

Fig. 2 Zeta potential of Fe_3O_4 nanoparticles, Fe_3O_4-PEI nanocomposites and clay minerals at different pH levels.

at 550 cm^{-1} and 580 cm^{-1}, which are assigned to the vibration of Fe–O bonds, were observed in both the coated and naked magnetic nanoparticles.[26] In the Fe_3O_4-PEI nanocomposite data, the peaks at 3245 and 1460 cm^{-1} correspond to N–H stretching vibrations,[27,28] while the bands at 2810 and 2915 cm^{-1} confirm the presence of aliphatic C–H stretching vibrations.[28] Therefore, these results clearly confirm the introduction of a PEI layer on the surface of the Fe_3O_4 nanoparticles.

The TGA weight-loss curves in Fig. S2† also demonstrate that PEI was successfully introduced on the surface of the magnetic nanoparticles. The Fe_3O_4-PEI nanocomposites underwent a weight loss of 13.9%, which was approximately 10% greater than that of the naked Fe_3O_4 nanoparticles (3.6%). Accordingly, the difference in weight loss between the Fe_3O_4-PEI nanocomposites and naked Fe_3O_4 nanoparticles was consistent with a mass ratio of 0.1 g-PEI per g-Fe_3O_4 nanoparticles.

PEI has a large number of amino groups that can capture protons at different pH values, known as the "proton sponge" mechanism.[29] As shown in Fig. 2, the PEI coating allowed the Fe_3O_4 nanoparticles to have a positive charge in the pH range of 2–10. In contrast, the surface charge of the clay minerals, including HBT, illite, kaolinite and montmorillonite, was mostly negative over a wide pH range. These results suggest that

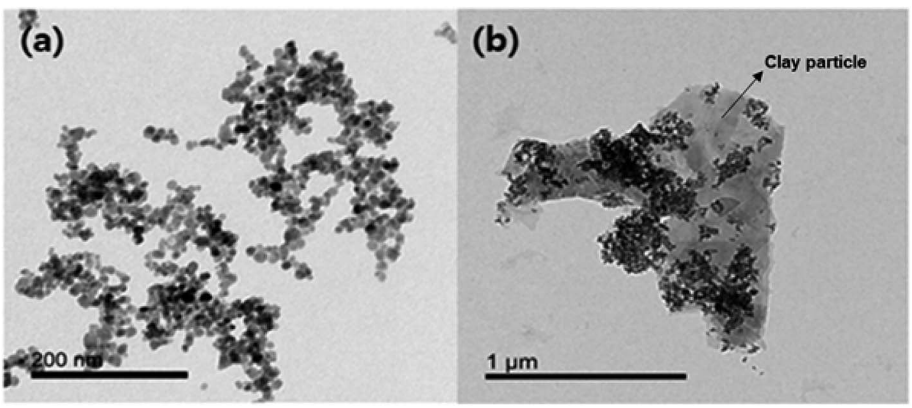

Fig. 1 TEM images of (a) Fe_3O_4-PEI nanocomposites and (b) Fe_3O_4-PEI nanocomposites adsorbed onto clay particles.

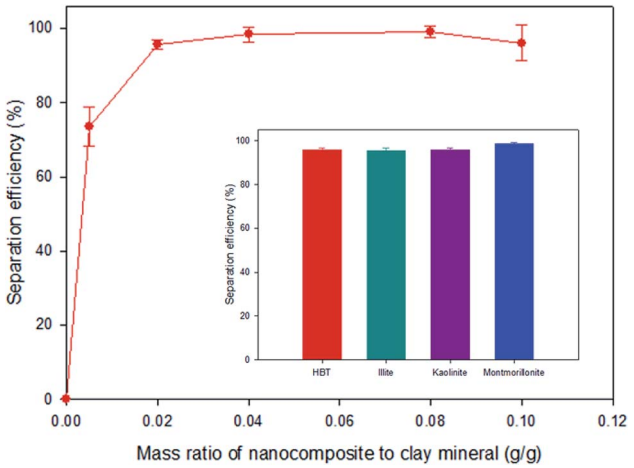

Fig. 3 Separation efficiency (SE) of HBT at pH 7 as a function of the mass ratio of Fe_3O_4-PEI nanocomposites to clay mineral. Inset compares SE of other clay minerals at a 0.02 g-Fe_3O_4-PEI nanocomposites per g-clay mineral.

the functionalized nanocomposites are likely to adsorb on the surface of clay minerals *via* electrostatic attraction under neutral conditions.

Interaction between the Fe_3O_4-PEI nanocomposites and clay minerals

Fig. 3 shows the SE of HBT from solution at mass ratios of the Fe_3O_4-PEI nanocomposites to HBT in the range of 0.005–0.100 at pH 7. The SE was 95.7% at 0.02 g-nanocomposite per g-clay, and the highest SE of approximately 100% was achieved when the mass ratio exceeded 0.04. Similarly, all clay minerals used for comparison showed a high SE of more than 95% at 0.02 g-nanocomposite per g-clay. These results suggested that the PEI coating improved the binding between the Fe_3O_4 nanoparticles and clay minerals, and thus, a high SE could be achieved at a low nanocomposite dose. A TEM image also clearly indicated that the Fe_3O_4-PEI nanocomposites were adsorbed on the surface of the clay particles (Fig. 1b).

The interaction mechanism between the Fe_3O_4-PEI nanocomposites and clay minerals was elucidated on the basis of charge neutralization (or the electrostatic patch mechanism) and electrostatic bridging.[30–33] The interaction of cationic Fe_3O_4 nanoparticles with oppositely charged clay particles leads to neutralization of their charges and destabilization of the system. Generally, negatively charged clay particles in solution are stably dispersed due to the electrostatic repulsion between them (Fig. S3†). However, after mixing the Fe_3O_4-PEI nanocomposites with clay particles, the cationic Fe_3O_4 nanoparticles strongly adsorbed onto the oppositely charged clay particles *via* a neutralization mechanism. As a result, the electrostatic repulsion between clay particles decreased, causing destabilization and coagulation. Charge neutralization plays a major role in magnetic flocculation by Fe_3O_4-PEI nanocomposites. In addition, the nanocomposites may adsorb onto the surface of clay particles *via* a bridging mechanism. Cationic Fe_3O_4-PEI nanocomposites can interact with negatively charged clay particles *via* the formation of a bridge between them, resulting in the formation of flocs. Therefore, the aggregation of colloid clay particles can be achieved through such interaction mechanisms involving Fe_3O_4-PEI nanocomposites. In the absence of a permanent magnet, it was confirmed that the clay particles that had reacted with the Fe_3O_4-PEI nanocomposites settled faster (within 120 s) than those that had reacted with naked Fe_3O_4 nanoparticles (Fig. S3†) because of the floc formation by the former particles.

Selective separation of fine particles from a soil mixture

To assess the selective separation of fine particles from soil, Fe_3O_4-PEI nanocomposites were mixed with a soil mixture containing 10% HBT at a mass ratio of 0.04 g-nanocomposite per g-HBT. Magnetic separation was then carried out with and without a mesh filter to account for the effects of sieving and nanocomposite dose on the selective separation of fine particles (Fig. 4). The results of magnetic separation are presented in accordance with the particle size distribution of the magnetic and nonmagnetic fractions of soil.

As shown in Fig. 5, the raw soil consisted of a 14% silt- and clay-sized fraction (<0.075 mm) and an 86% sand-sized fraction (0.075–2 mm). Without the mesh filter, the separated magnetic soil fraction accounted for 18.9%, and this fraction was found to

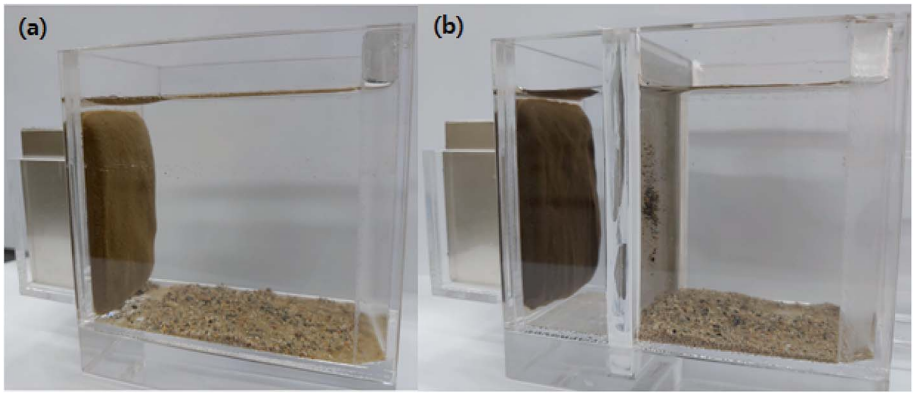

Fig. 4 Photographs of magnetic separation (a) without a mesh filter and (b) with a mesh filter (magnetic field strength is 0.38 T).

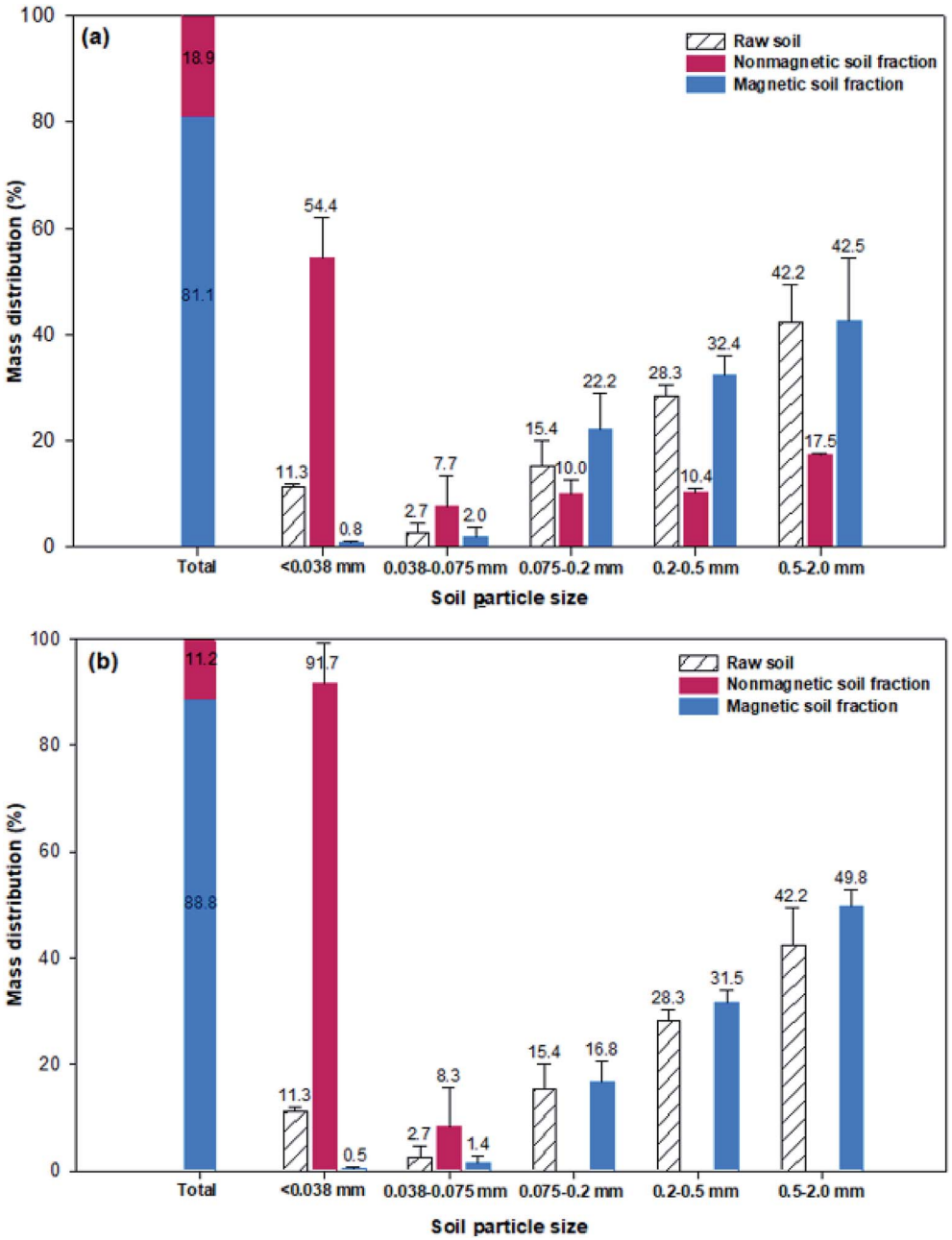

Fig. 5 Particle size distributions after magnetic separation (a) without a mesh filter and (b) with a mesh filter.

consist of 54.4% fine particles smaller than 0.038 mm, 7.7% silt-sized particles (0.038–0.075 mm) and 37.9% sand-sized particles. Although most of the fine particles were magnetically separated, some sand-sized particles were also present, so the addition of a mesh filter was expected to increase the SE; the results are shown in Fig. 5b. Upon the addition of the mesh filter, the fine particles in the magnetic soil fraction became the predominant fraction, with a proportion of 91.7%, because the sand-sized particles did not pass through the mesh filter. Moreover, the sand-sized fraction made up 98.1% of the nonmagnetic soil fraction, which suggests that most of the fine soil particles were collected in the magnetic part. Therefore, the combination of magnetic separation with a mesh filter enabled more thorough separation of fine particles from the soil mixture, ultimately reducing the volume of magnetic soil (*i.e.*, Cs-enriched soil) from 18.9% to 11.2%.

In addition, the effects of different nanocomposite doses (0.04, 0.08, 0.12, and 0.16 g-nanocomposite per g-HBT) on the SE of fine particles are compared in Fig. 6. The SE increased slightly with an increase in the dose of Fe_3O_4-PEI nanocomposite, and the highest SE was approximately 99.3%, obtained at a mass ratio of 0.16 g g^{-1}. In the case of silt-sized particles (0.075–0.038 mm), the increase in SE with increasing nanocomposite dose was greater than that for the other particle sizes and remained above

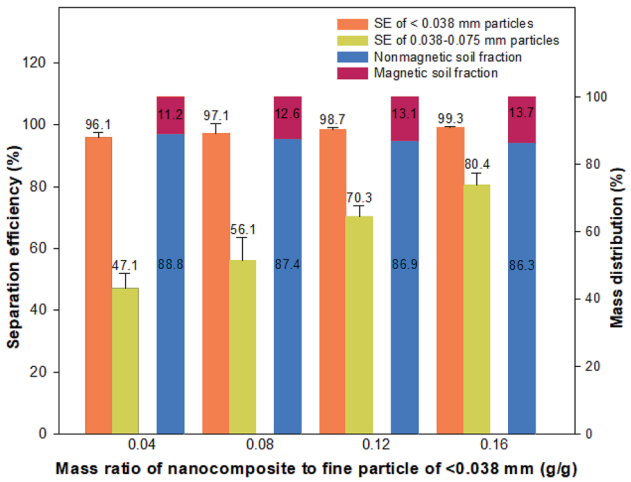

Fig. 6 The effect of Fe_3O_4-PEI nanocomposites dosage on separation efficiency of fine particles.

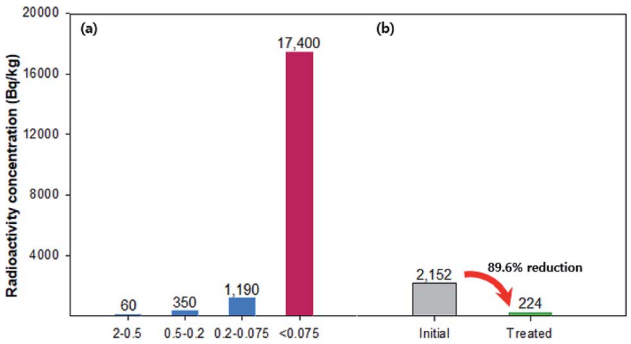

Fig. 7 A radioactivity of (a) the raw soil according to the four size fraction; 2–0.5, 0.5–0.2, 0.2–0.075, and <0.075 mm, (b) initial value and treated value using magnetic-sieving separation.

0.12 g g^{-1}. Therefore, it was concluded that a nanocomposite dose of 0.12 g g^{-1} is suitable for magnetic-sieving separation of silt- and clay-sized fine particles.

Evaluation of the ^{137}Cs radioactivity reduction in contaminated soil

To demonstrate the effect of magnetic-sieving separation on the remediation of radioactive soil, ^{137}Cs-contaminated soil was reacted with Fe_3O_4-PEI nanocomposites at a mass ratio of approximately 1.2% of the contaminated soil. The initial radioactivity of the ^{137}Cs-sorbed soil was 2152 Bq kg^{-1}. As shown in Fig. 7, to examine the particle size dependence of ^{137}Cs radioactivity, the raw soil was separated into four fractions: 2–0.5 mm, 0.5–0.2 mm, 0.2–0.075 mm, and <0.075 mm. The ^{137}Cs radioactivity distribution revealed a high Cs concentration in the fine fraction (17 400 Bq kg^{-1} in the <0.075 mm portion). After magnetic-sieving separation, the treated nonmagnetic fraction, which accounted for 87.5% of the total soil, had a value of 224 Bq kg^{-1} (10.4% of the total ^{137}Cs). These results suggest that a high decontamination efficiency of approximately 90% was achieved by simple physical separation of fine soil particles without additional chemical treatment.

In Cs-contaminated soil from the nuclear accident sites of Chernobyl and Fukushima, the distribution of radioactivity among the various soil particle sizes was analyzed, and it was confirmed that higher radioactivity is found in smaller particles.[34,35] Therefore, methods to separate highly contaminated fine particles from soil are possible soil decontamination strategies. Although several studies have considered chemical separation alone using flotation or magnetic methods for Cs-contaminated soil treatment,[20–23] such methods cannot be implemented in practice (Table 1). Thus, our results have demonstrated that magnetic-sieving separation using Fe_3O_4-PEI nanocomposites is an effective method to decontaminate radioactive soil.

Conclusion

The aim of this work was to increase the selectivity of the separation of Cs-enriched clay particles from contaminated soil by combining magnetic and sieving methods. Fe_3O_4-PEI

Table 1 Comparison of separation methods in Cs-contaminated soil treatment

Method	Object	Results	Advantages	Disadvantages	Reference
Magnetic separation with Fe_3O_4-PEI nanocomposites	Selective separation of Cs-fine particles from soil	Reduction of radioactivity: 89.6% Reduction of volume: 80%	Simple operation, low energy consumption, high decontamination rate	High cost of nanocomposite synthesis	This study
Magnetic separation with nano-Fe/Ca/CaO/$[PO_4]$ under dry condition	Separation and immobilization of Cs in contaminated soil	Reduction of radioactivity: 88.1% Reduction of volume: 72.8%	High decontamination rate, no water use	High cost of nanocomposite synthesis	23
Magnetic separation with superconducting magnet	Separation of 1 : 1 and 2 : 1 type clay mineral	Reduction of radioactivity: 20%	Simple process	Low separation efficiency, high energy consumption	22
Foam flotation with EDAB	Separation of Cs-clay from pristine clay (montmorillonite)	Separation efficiency of contaminated clay: 75%	Ease of scale up, high separation efficiency	Limitation of applicability, generation of wastewater	21
Foam flotation with TTAB	Selective separation of Cs-fine particles from soil	Separation efficiency: 55% of 2–20 μm, 58.5% of 20–50 μm, 47% of 50–100 μm	Ease of scale up, high separation efficiency	Poor separation efficiency of clay particles, generation of wastewater	20

nanocomposites were selectively adsorbed onto negatively charged clay particles *via* electrostatic interactions over a wide pH range. The synthesized functionalized nanocomposites enhanced the binding force between the Fe_3O_4 nanoparticles and clay minerals; thus, almost 100% of clay particles were separated from solution with a low nanocomposite dose. The combination of magnetic separation with a mesh filter also showed that fine particles could be more selectively separated from a soil mixture by excluding sand-sized particles. In addition, magnetic-sieving separation effectively led to a reduction in radioactivity of approximately 90% in ^{137}Cs-contaminated soil. Therefore, the combined application of Fe_3O_4-PEI nanocomposites and a mesh filter for the selective separation of clay particles may provide new insights for the design of novel practical technologies for the remediation of radioactive soil.

Conflicts of interest

There are no conflicts to declare.

Acknowledgements

This work was supported by the National Research Foundation of Korea (NRF) grant funded by the Korean government, Ministry of Science and ICT (No. 2017M2A8A5015148).

References

1 T. J. Yasunari, A. Stohl, R. S. Hayano, J. F. Burkhart, S. Eckhardt and T. Yasunari, Cesium-137 deposition and contamination of Japanese soils due to Fukushima nuclear accident, *Proc. Natl. Acad. Sci. U.S.A.*, 2011, **108**, 19530–19534.

2 A. Bugger and I. Lichtscheidl, Stable and radioactive cesium: a review about distribution in the environment, uptake and translocation in plants, plant reactions and plants' potential for bioremediation, *Sci. Total Environ.*, 2018, **618**, 1459–1485.

3 J. Takahashi, S. Wakabayashi, K. Tamura and Y. Onda, Downward migration of radiocesium in an abandoned paddy soil after the Fukushima Dai-ichi nuclear power plant accident, *J. Environ. Radioact.*, 2018, **182**, 157–164.

4 X. Yin, L. Zhang, C. Meng, Y. Inaba, X. Wang, A. Nitta, Y. Koma and K. Takeshita, Selective removal of radiocesium from micaceous clay for post-accident soil decontamination by temperature-controlled Mg-leaching in a column, *J. Hazard. Mater.*, 2020, **387**, 121677.

5 M. Okumura, S. Kerisit, I. C. Bourg, L. N. Lammers, T. Ikeda, M. Sassi, K. M. Rosso and M. Machida, Radiocesium interaction with clay minerals: theory and simulation advances Post-Fukushima, *J. Environ. Radioact.*, 2018, **189**, 135–145.

6 B. L. Sawhney, Potassium and cesium ion selectivity in relation to clay mineral structure, *Clay Clay Miner.*, 1970, **18**, 47–52.

7 B. L. Sawhney, Selective sorption and fixation of cations by clay minerals: a review, *Clay Clay Miner.*, 1972, **20**, 93–100.

8 C. W. Francis and F. S. Brinkley, Preferential adsorption of ^{137}Cs to micaceous minerals in contaminated freshwater sediment, *Nature*, 1976, **260**, 511–513.

9 J. M. Zachara, S. C. Smith, C. Liu, J. P. McKinley, R. J. Serne and P. L. Gassman, Sorption of Cs^+ to micaceous subsurface sediments from the Hanford site, USA, *Geochim. Cosmochim. Acta*, 2002, **66**, 193–211.

10 L. K. Zaunbrecher, R. T. Cygan and W. C. Elliott, Molecular models of cesium and rubidium adsorption on weathered micacesous minerals, *J. Phys. Chem. A*, 2015, **119**, 5691–5700.

11 I. Kim, J. H. Kim, S. M. Kim, C. W. Park, I. H. Yoon, H. M. Yang and K. W. Lee, Desorption of cesium from hydrobiotite by hydrogen peroxide with divalent cations, *J. Hazard. Mater.*, 2020, **390**, 121381.

12 H. Mukai, T. Hatta, H. Kitazawa, H. Yamada, T. Yaita and T. Kogure, Speciation of radioactive soil particles in the Fukushima contaminated area by IP autoradiography and microanalyses, *Environ. Sci. Technol.*, 2014, **48**, 13053–13059.

13 H. Mukai, K. Tamura, R. Kikuchi, Y. Takahashi, T. Yaita and T. Kogure, Cesium desorption behavior of weathered biotite in Fukushima considering the actual radioactive contamination level of soils, *J. Environ. Radioact.*, 2018, **190–191**, 81–88.

14 D. W. Evans, J. J. Alberts and R. A. Clark III, Reversible ion-exchange fixation of cesium-137 leading to mobilization from reservoir sediments, *Geochim. Cosmochim. Acta*, 1983, **47**, 1041–1049.

15 C. B. Durrant, J. D. Begg, A. B. Kersting and M. Zavarin, Cesium sorption reversibility and kinetics on illite, montmorillonite, and kaolinite, *Sci. Total Environ.*, 2018, **610–611**, 511–520.

16 T. Kogure, K. Morimoto, K. Tamura, H. Sato and A. Yamagishi, XRD and HRTEM evidence for fixation of cesium ions in vermiculite clay, *Chem. Lett.*, 2012, **41**, 380–382.

17 K. Sato, K. Fujimoto, W. Dai and M. Hunger, Molecular mechanism of heavily adhesive Cs: why radioactive Cs is not decontaminated from soil, *J. Phys. Chem. C*, 2013, **117**, 14075–14080.

18 H. Kato, Y. Onda and M. Teramage, Depth distribution of ^{137}Cs, ^{134}Cs, and ^{137}I in soil profile after Fukushima Dai-ichi nuclear power plant accident, *J. Environ. Radioact.*, 2012, **111**, 59–64.

19 T. M. Nakanishi, Agricultural implications of the Fukushima nuclear accident, *J. Radiat. Res.*, 2016, **57**, i47–i52.

20 A. B. Said, F. Frances, A. Grandjean, C. Latrille and S. Faure, Study of a foam flotation process assisted by cationic surfactant for the separation of soil clay particles: processing parameters and scaling-up sensitivity, *Chem. Eng. Process.*, 2019, **142**, 107547.

21 H. Zhang, S. Tangparitkul, B. Hendry, J. Harper, Y. K. Kim, T. N. Hunter, J. W. Lee and D. Harbottle, Selective separation of cesium contaminated clays from pristine clays by flotation, *Chem. Eng. J.*, 2019, **355**, 797–804.

22 S. Igarashi, N. Nomura, F. Mishima, Y. Akiyama and S. Nishijima, Study on magnetic separation for

decontamination of cesium contaminated soil by using superconducting magnet, *Physica C*, 2014, **504**, 144–147.

23 S. R. Mallampati, Y. Mitoma, T. Okuda, C. Simion and B. K. Lee, Solvent-free synthesis and application of nano-Fe/Ca/CaO/[PO_4] composite for dual separation and immobilization of stable and radioactive cesium in contaminated soils, *J. Hazard. Mater.*, 2015, **297**, 74–82.

24 J. H. Kim, S. M. Kim, I. H. Yoon, S. J. Choi and I. Kim, Selective separation of Cs-contaminated clay from soil using polyethylenimine-coated magnetic nanoparticles, *Sci. Total Environ.*, 2020, **706**, 136020.

25 S. Ge, M. Agbakpe, Z. Wu, L. Kuang, W. Zhang and X. Wang, Influences of surface coating, UV irradiation and magnetic field on the algae removal using magnetite nanoparticles, *Environ. Technol.*, 2015, **49**, 1190–1196.

26 Y. Z. Wu, M. Chen, X. H. Yan, J. Ren, Y. Dai, J. J. Wang, J. M. Pan, Y. P. Wang and X. N. Cheng, Hydrothermal synthesis of Fe_3O_4 nanorods/graphitic C_3N_4 composite with enhanced supercapacitive performance, *Mater. Lett.*, 2017, **198**, 114–117.

27 I. Karimazadeh, M. Aghazadeh, M. R. Ganjali, T. Doroudi and P. H. Koilvand, Preparation and characterization of iron oxide (Fe_3O_4) nanoparticles coated with polyvinylpyrrolidone/polyethylenimine through a facile one-pot deposition route, *J. Magn. Magn. Mater.*, 2017, **433**, 148–154.

28 A. Kasprzak, M. Popławska, M. Bystrzejewski, O. Łabędź and I. P. Grudziński, Conjugation of polyethylenimine and its derivatives to carbon-encapsulated iron nanoparticles, *RSC Adv.*, 2015, **5**, 85556–85567.

29 K. Gerulová, A. Bartošová, L. Bartošová, K. Bártová, M. Dománková, Z. Garaiová and M. Palcut, Magnetic Fe_3O_4-polyethyleneimine nanocomposites for efficient harvesting of Chlorella zofingiensis, Chlorella vulgaris, Chlorella sorokiniana, Chlorella ellipsoidea and Botryococcus braunii, *Algal Res.*, 2018, **33**, 165–172.

30 D. Vandamme, I. Foubert and K. Muylaert, Flocculation as a low-cost method for harvesting microalgae for bulk biomass production, *Trends Biotechnol.*, 2013, **31**, 233–239.

31 G. P. Lam, M. H. Vermuë, G. Olivieri, L. A. M. van den Broek, M. J. Barbosa, M. H. M. Eppink, R. H. Wijffels and D. M. M. Kleinegris, Cationic polymers for successful flocculation of marine microalgae, *Bioresour. Technol.*, 2014, **169**, 804–807.

32 S. B. Ummalyma, E. Gnansounou, R. K. Sukumaran, R. Sindhu, A. Pandey and D. Sahoo, Bioflocculation: an alternative strategy for harvesting of microalgae-An overview, *Bioresour. Technol.*, 2017, **242**, 227–235.

33 I. Branyikova, G. Prochazkova, T. Potocar, Z. Jezkova and T. Branyik, Harvesting of microalgae by flocculation, *Fermentation*, 2018, **4**, 1–12.

34 M. Kaneko, H. Iwata, H. Shiotsu, S. Masaki, Y. Kawamoto, S. Yamasaki, Y. Nakamatsu, J. Imoto, G. Furuki, A. Ochiai, K. Nanba, T. Ohnuki, R. C. Ewing and S. Utsunomiya, Radioactive Cs in the severely contaminated soils near the Fukushima Daiichi nuclear power plant, *Front. Energy Res.*, 2015, **3**, 37.

35 J. Koarashi, S. Nishimura, M. Atarashi-Andoh, T. Matsunaga, T. Sato and S. Nagao, Radiocesium distribution in aggraegate-size fractions of cropland and forest soils affected by the Fukushima nuclear accident, *Chemosphere*, 2018, **205**, 147–155.